ISSN 1027-5495. Functional Materials, 25, No.1 (2018), p. 67-74.
doi:https://doi.org/10.15407/fm25.01.67

Investigation of structural, textural, optical and photocatalytic properties of Sn/TiO_2 nanocomposites

***T.A.Khalyavka*[1], *S.V.Camyshan*[1], *L.A.Davydenko*[2], *V.V.Permyakov*[3], *S.N.Shcherbakov*[4]**

[1]Institute for Sorption and Problems of Endoecology, National Academy of Sciences of Ukraine, 13 General Naumov Str., 03164 Kyiv, Ukraine
[2]Chuiko Institute of Surface Chemistry, National Academy of Sciences of Ukraine, 17 General Naumov Str., 03164 Kyiv, Ukraine
[3]Institute of Geological Sciences, National Academy of Sciences of Ukraine, 55-b O.Gonchar Str., 01054 Kyiv, Ukraine
[4]M.Kholodny Institute of Botany, National Academy of Sciences of Ukraine, 2 Tereshenkivska Str., MSP-1, 01601 Kyiv, Ukraine

Received June 5, 2017

Nanoscale composite materials based on titanium dioxide and tin were obtained. The obtained powders were characterized by XRD, EDS, SEM, TEM, BET and UV-VIS spectroscopy. The XRD spectrum reveals anatase and rutile structure. Increasing the amount of tin in the composites leads to increase of crystallite size, lattice parameters, pore radius and decrease of specific surface area and pore volume. Analysis of nitrogen sorption-desorption isotherms for the synthesized samples showed the presence of a hysteresis loop which is the evidence for mesoporous structure of the powders. Absorption spectra of the nanocomposites showed a bathochromic shift as compared with pure TiO_2. It was found that tin additives leads to band gap narrowing of TiO_2. Photocatalytic activity of some cationic dyes (Safranin T, Rhodamine C) under UV and visible irradiation in the presence of composites of Sn/TiO_2 was investigated. The composite samples were photocatalytically active in destruction of the cationic dyes in water solutions under UV and visible irradiation. It may be connected with the narrowing of band-gap width, participation of tin in inhibition of electron-hole recombination, prolongation of charges lifetime, increasing of efficiency of interfacial charge separation from TiO_2 to tin and formation of doping electronic states.

Keywords: titanium dioxide, tin, composites, photocatalysis, dyes.

Получены наноразмерные композитные материалы на основе диоксида титана и олова. Рентгенофазовый анализ показал наличие фазы анатаза и рутила во всех образцах. Выявлено, что с увеличением количества олова в композитах размеры кристаллитов, параметры решетки и радиус пор увеличиваются, а удельная поверхность и объем пор уменьшаются. Исследование изотерм сорбции-десорбции азота для синтезированных порошков показало наличие петли гистерезиса, что свидетельствует об их мезопористой структуре. В спектрах поглощения нанокомпозитов наблюдается батохромный сдвиг по сравнению с чистым TiO_2. Установлено, что добавки олова приводят к уменьшению ширины запрещенной зоны TiO_2. Исследована фотокаталитическая деструкция катионных красителей (сафранин Т, родамин С) при воздействии облучения ультрафиолетовым и видимым светом в присутствии мезопористых нанокомпозитов Sn/TiO_2. Композитные образцы оказались более фотокаталитически активными в деструкции

катионных красителей в водных растворах под воздействием облучения ультрафиолетовым и видимым светом по сравнению с чистым диоксидом титана. Это может быть связано с сужением ширины запрещенной зоны, с участием олова в ингибировании процесса рекомбинации электронов и дырок, пролонгированием жизни зарядов, с увеличением эффективности разделения зарядов на границе раздела фаз, а также с формированием дополнительных электронных уровней.

Дослідження структурних, текстурних, оптичних та фотокаталітичних властивостей Sn/TiO_2 нанокомпозитів. *Т.О. Халявка, С.В.Камишан, Л.О.Давиденко, В.В.Пермяков, С.М.Щербаков*

Одержано нанорозмірні композитні матеріали на основі діоксиду титану та олова. Порошки охарактеризовано з використанням методів РФА, СЕМ, ТЕМ, ВЕТ, УФ та видимої спектроскопії. Рентгенофазовий аналіз показав наявність фази анатазу та рутилу в усіх зразках. Виявлено, що зі збільшенням кількості олова у композитах відбувається збільшення розмірів кристалітів, параметрів гратки, радіусу пор та зменшення питомої поверхні і об'єму пор. Дослідження ізотерм сорбції-десорбції азоту для синтезованих порошків показало наявність петлі гістерезису, що свідчить про їх мезопорувату структуру. У спектрах поглинання нанокомпозитів спостерігається батохромний зсув у порівнянні з чистим TiO_2. Встановлено, що добавки олова призводять до зменшення ширини забороненої зони TiO_2. Досліджено фотокаталітичну деструкцію катіонних барвників (сафранін Т, родамін С) під дією опромінювання ультрафіолетовим та видимим світлом за присутності мезопоруватих нанокомпозитів Sn/TiO_2. Композитні зразки виявилися більш фотокаталітично активними у деструкції катіонних барвників у водних розчинах під дією опромінювання ультрафіолетовим та видимим світлом у порівнянні з чистим діоксидом титану. Це може бути пов'язаним зі звуженням ширини забороненої зони, з участю олова в інгібуванні процесу рекомбінації електронів та дірок, подовженням життя зарядів, зі збільшенням ефективності розділення зарядів на межі розділу фаз, а також з формуванням додаткових електронних рівнів.

1. Introduction

Titanium dioxide is a widely used photocatalyst, however, it has several serious disadvantages: insufficiently high quantum yield of the reaction, wide band gap (3.2 eV), high rate of electron-hole recombination, and peculiarity of light adsorption by TiO_2 resulting in its photochemical activity only in UV region of spectrum. But ultraviolet light occupies only 4 % of sunlight; on the other hand, visible light accounts about 43 %. Thus, it seems more practical and favorable to use the visible light rather than ultraviolet light for the degradation process. So, an urgent problem in photocatalysis is a search for photocatalytic systems which are active under visible light irradiation that gives an opportunity of their widespread practical application.

Researchers try to shift the optical sensitivity of TiO_2 from the UV to the visible-light region and to decrease the band gap and rate of electron-hole recombination for the efficient use of solar energy by many methods, such as metal loading, doping and coupling of composite semiconductors [1–4].

Combining semiconductors give one of the ways to solve the above mentioned problems. Besides, the study of semiconductor nanoparticles attracts attention of researchers because of their unique optical and electrical properties. In recent years, scientists started to focus on Sn/TiO_2 system. For example, R.M.Mohamed et al. used TiO_2 nanospheres, doped by tin for aniline synthesis [1], D.Nithyadevi et al. investigated the properties of TiO_2–SnO_2 composite nanoparticles [5], Y.Zhao et al. received uniform $Ti_{1-x}Sn_xO_2$ nanocrystal colloids [6], I.Rangel-Vazquez et al. examined Sn doped TiO_2 photocatalysts for photocatalytic degradation of 2,4-dichlorophenoxyacetic acid [7].

As we know, SnO_2 is an optoelectrical *n*-type semiconductor, as well as TiO_2. The band gap energy level of SnO_2 is higher than that of TiO_2; the conduction band of SnO_2 is at a lower level than that of TiO_2. The higher reduction power of electrons and the higher oxidation power of holes correspond to the higher position of conduction band and the lower position of valence band, respectively. Therefore, combining two semiconductors with different energy levels for their corresponding conduction and valence bands can provide an approach to achieve better applications by increasing the efficiency of charge separation, charge carrier lifetime, interfacial charge transfer rate and extending the energy range of photoexcitation [8, 9].

So, the aim of our work was to prepare nanosized Sn/TiO_2 composites with photo-

catalytic activity under visible light irradiation and investigation the influence of tin and its amount on structural, textural, optical and photocatalytic properties of the composites.

2. Experimental

2.1. Preparation of composites

Oxide titanium-tin composites were obtained through calcination of mixtures of titanium (IV) tetrabutoxide (Aldrich), citric acid, castor oil and $SnCl_2$ (0.1, 0.5, 1, and 2 g) [10]. The samples designated as $0.1Sn/TiO_2$, $0.5Sn/TiO_2$, $1Sn/TiO_2$, and $2Sn/TiO_2$, respectively, were prepared by annealing of each mixture at 500°C during 2 h in the presence of air oxygen. Before annealing, the mixture was carefully stirred up to yield uniform mass. One more TiO_2 sample was prepared using the above procedure without addition of $SnCl_2$.

2.2. Characterization of photocatalysts

The prepared photocatalysts were fully characterized by powder XRD to verify their crystalline structure using diffractometer Dron-4-07 (Russia) at CuKα radiation (with a copper anode and nickel filter) in reflection beam and the Bragg-Brentano registration geometry (2θ= 10–70°). All XRD peaks were checked and assigned to known crystalline phases. Average crystallite size was determined using broadening of the most intensive band by means of the Debye-Scherrer equation [11]:

$$D = 0.9\lambda/B\cos\theta,$$

where 0.9 is a constant, λ is a wavelength, nm. Crystalline sizes were determined through characteristics of the most intensive peaks. Interplanar distance (d, nm) was calculated using the Wulff-Bragg's equation: $n\lambda = 2d\sin\theta$, where $n = 1$ is the order of reflection, $\lambda = 0.154$ nm is the wavelength, θ is the scattering angle, degrees. Thereby, $d = n\lambda/2\sin\theta$.

Diffuse reflectance spectra of the powders were measured using Perkin-Elmer Lambda Bio 35 spectrophotometer in the range between 200 and 1000 nm which allows one to convert data of corresponding spectra using the Kubelka-Munk equation. The band gap value (E_g) was calculated according to [12] using the following formula: $E_g = 1239.8/\lambda$ where λ (nm) is the wavelength of absorption edge in the spectrum.

To analyze the sample composition (elemental analysis) and its morphology a scanning electron microscope (SEM JSM 6490 LV, JEOL, Japan) with an integrated system for electron microprobe analysis INCA Energy based on energy-dispersive and wavelength-dispersive spectrometers (EDS + WDS, OXFORD, United Kingdom) with HKL Channel system was used.

Transmission electron microscopy (TEM) for received material was carried on a transmission electron microscope JEM-1200 EX (JEOL, Japan).

The values of specific surface (S_{sp}) of the samples as well as distribution of pores by volume were determined using Quantachrom NovaWin2 device. The specific surface of the samples was obtained from isotherms of nitrogen sorption-desorption using the Brunauer-Emmet-Teller (BET) approach [13]. The pore radius (R) and the pore volume (V_{tot}) were calculated from desorption branches of the isotherms using the Barret-Joiner-Halenda method [14].

2.3 Photocatalytical experiment

We choose cationic dyes safranin T (ST) ($C = 0.03$ g/l) and rhodamine C (RB) (C = 0.03 g/l) as models of pollutants to evaluate the composites degradation activity under visible light irradiation, because these dyes are widely applied, are stable under visible irradiation and difficult for biodegradation.

Photocatalytic activity of the samples was evaluated by rate constants of destruction (k_d) of the models. Before irradiation, catalyst suspension (2 g/l) in aqueous substrate solution was left in dark up to achieve the adsorption equilibrium. Irradiation of aqueous solutions of these dyes was performed at room temperature in a quartz reactor in the presence of air oxygen. As a light source we used a high-intensity Na discharge lamp GE Lucalox (Hungary) with power of 70 W, the latter emitting in the visible region with maxima at 568, 590 and 600 nm.

Concentrations of the substrates were measured by spectrophotometric technique using Shimadzu UV-2450 spectrophotometer at $\lambda = 520$ nm for SF and $\lambda = 552$ nm for RD. Photocatalytic rate constants for the model compounds were calculated using the pseudo-first-order kinetics equation [15].

3. Results and discussion

Investigation of the obtained powders by means of energy-dispersive spectroscopy based on energy-dispersive technique proves

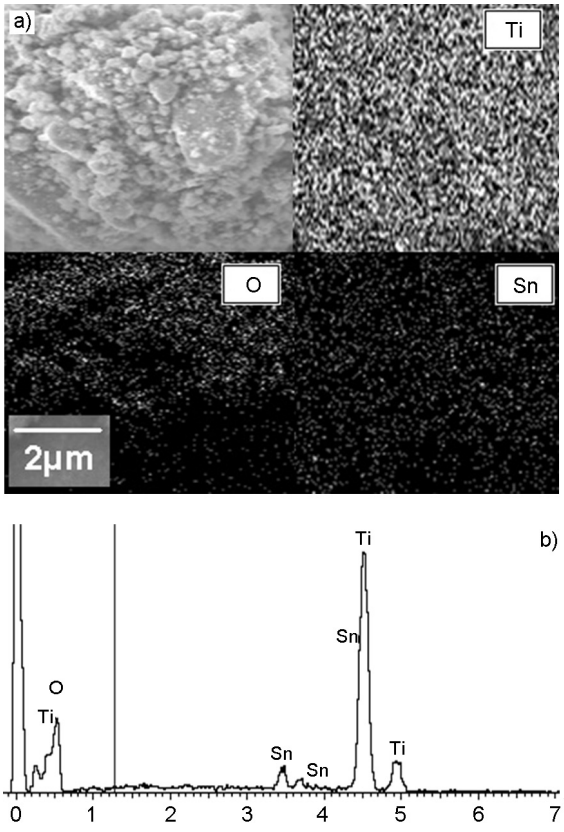

Fig. 1. Energy-dispersive spectrometry (EDS) spectrum and EDS elemental mapping of $0.1Sn/TiO_2$.

that these materials include Ti, O, and Sn elements, no unexpected elements being detected (Fig. 1).

Weight content of Sn in the range from $0.1Sn/TiO_2$ to $2Sn/TiO_2$ enhances from 7.21, 9.64, 11.43 to 14.35 %, respectively. The EDS elemental mappings from a selected area show that atoms of Sn, O and Ti are distributed evenly and uniformly in the samples (Fig. 1).

Crystalline structure of the photocatalysts was identified by using XRD. Diffractogram of pure titanium dioxide shows intensive peaks at $2\theta = 25.4$; 37.8; 48.0, which belongs to anatase phase and at $2\theta = 27.4$; 41.2; 54.2; 56.7 characteristic of rutile phase (Fig. 2, a). All the composite samples revealed weak peaks at $2\theta = 25.4$; 38.94; 48.2, which belong to the anatase phase (Fig. 2, a) and intense peaks corresponding to the rutile phase at $2\theta = 26.76$, 34.04, 38.12, 51.92, 54.2, 62.12, 64.8 and 66.2.

In contradiction to results of the works [5, 7] the peaks characteristic of brookite phase, were not found. It is known [16–18], that additives of Cd, Au, Mn and Ag enhance the powders crystallization and promote the transition of the anatase to rutile. Thus, intensive peaks of the rutile were discovered in all the samples. It should be pointed out that addition of tin and further increase of its content in the powders led to shifting of the rutile peaks to lesser angles 2θ to the position of SnO_2 rutile (Fig. 2, a). This may be explained by substitution of Ti^{4+} ions with Sn^{4+} ions in the crystal lattice, because Ti^{4+} ion radius (53 nm) is close to the tin ion radius (69 nm) [1]. The anatase peaks are not shifted as tin content increases. Besides, tin oxide has a tetragonal crystal system with the rutile structure, but lattice constants of SnO_2 rutile are greater than those of TiO_2 rutile. As a result, introduction of tin into titanium dioxide should lead to the lattice expansion, i. e.

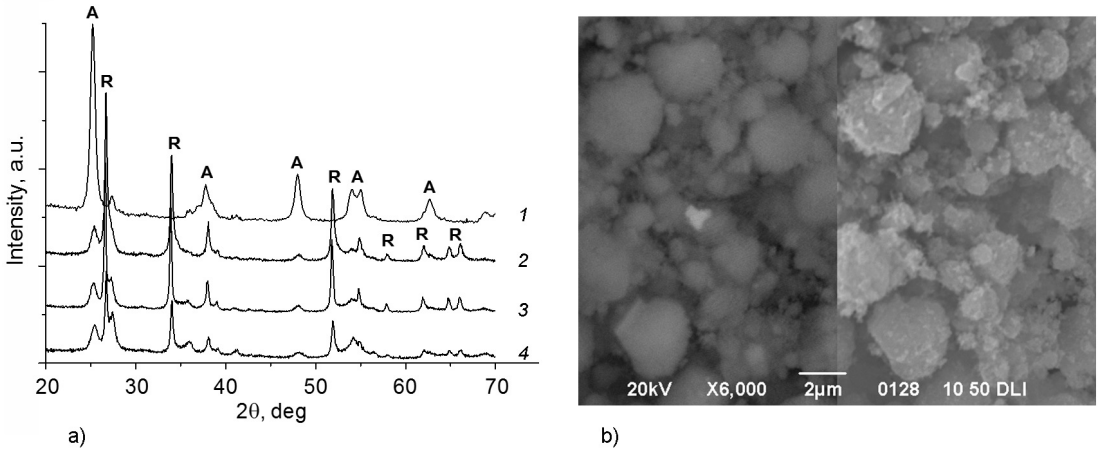

Fig. 2. a: XRD spectra for: *1* — TiO_2, *2* — $2Sn/TiO_2$, *3* — $1Sn/TiO_2$, *4* — $0.5Sn/TiO_2$ (A — anatase, R — rutile), b: SEM-images of the $0.1Sn/TiO_2$ sample in secondary electrons mode (right) and reflected electrons (left).

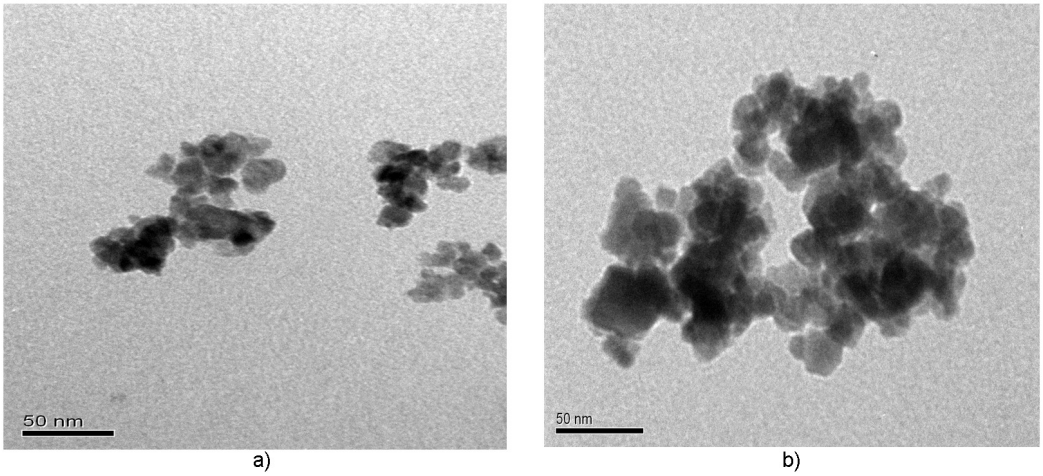

Fig. 3. TEM-images: a — TiO_2, b — $0.5Sn/TiO_2$ sample.

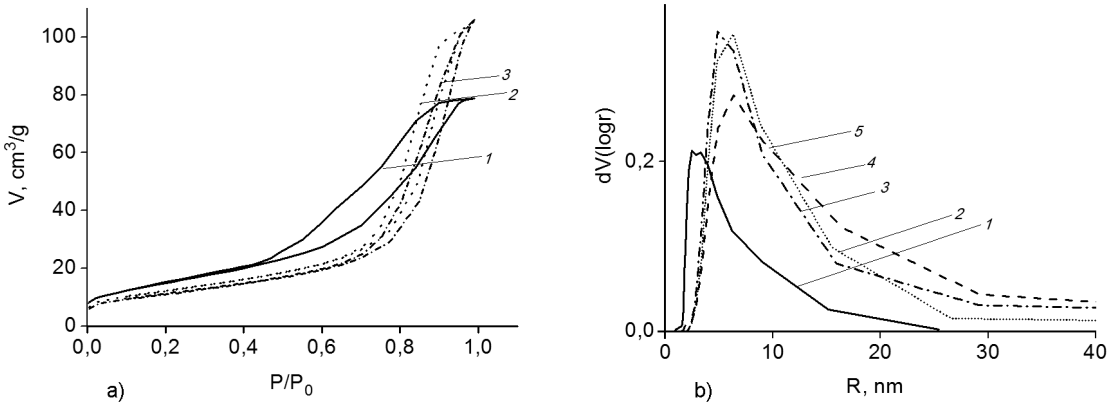

Fig. 4. a) Isotherms of nitrogen sorption-desorption obtained at 20°C for some investigated samples: *1* — TiO_2, *2* — $1Sn/TiO_2$, *3* — $2Sn/TiO_2$; b) Pore size distribution for the samples: *1* — TiO_2, *2* — $0.1Sn/TiO_2$, *3* — $0.5Sn/TiO_2$, *4* — $1Sn/TiO_2$, *5* — $2Sn/TiO_2$ (b).

to increase of TiO_2 lattice parameters [19]. Indeed, the lattice parameters of the composite samples increase as compared with pure titanium oxide.

Analysis of SEM-images of the samples shows that they consist of roundish agglomerates (Fig. 2, b). Crystallite size in the agglomerates of titanium dioxide as calculated through the Debye-Scherrer equation equals to 11.68 nm (anatase 101) and 7.67 nm (rutile 110). In the case of composite samples are in the range from $0.5Sn/TiO_2$ to $2Sn/TiO_2$ their values increase from 6.06 to 7.60 nm (anatase 101) and from 21.41 to 30.72 nm (rutile 110). This is supported by the studies using TEM (Fig. 3).

Analysis of nitrogen sorption-desorption isotherms obtained at 20°C for the synthesized samples (Fig. 4, a) shows the presence of a hysteresis loop which is the evidence for mesoporous structure of the powders [20]. The isotherms correspond to type IV of IUPAC classification for mesoporous materials with H1 type of the hysteresis loop [21]. Predominance of the pores up to 10 nm is characteristic of pure titanium dioxide, whereas for the composite samples this value is 5–20 nm (Fig. 4, b).

Specific surface area of the samples falls from 47.56 to 40.0 m^2/g with increasing of tin content (Table 1). These results are in accordance with the XRD data, because the enhancement of tin content leads to rise of crystallite size in the both phases, leading to decrease of the specific surface area of the samples.

Mean pore volume and radius of pores in the composite samples are greater than those in pure titanium dioxide (Table 1). In the range of the samples from $0.1Sn/TiO_2$ to $2Sn/TiO_2$ the mean pore volume decrease from 0.2 to 0.164 cm^2/g, whereas the mean pore radius increase from 7.91 to 8.2 nm, which is in accordance with the fact of en-

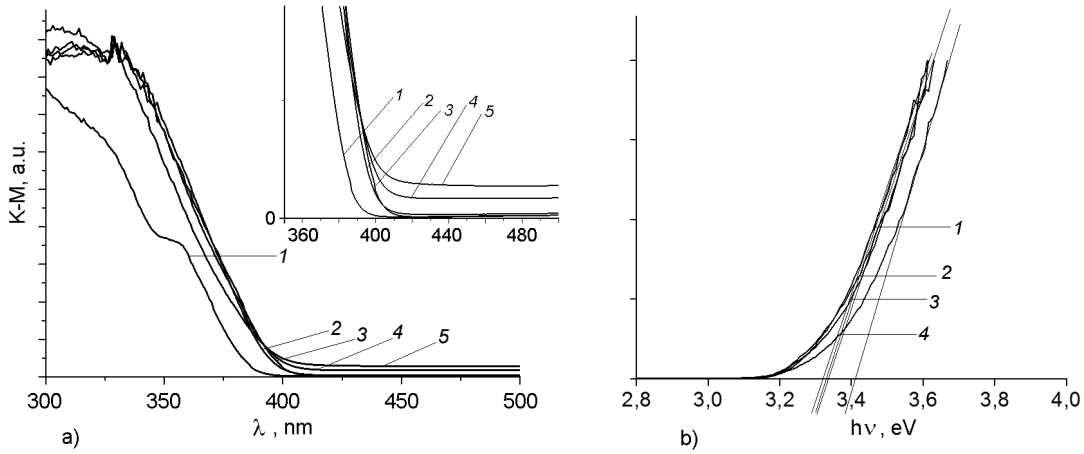

Fig. 5. a) UV-Vis diffuse reflectance spectra of samples: *1* — TiO_2, *2* — $0.1Sn/TiO_2$, *3* — $0.5F2Sn/TiO_2$, *4* — $1Sn/TiO_2$, *5* — $2Sn/TiO_2$; b) Square of extinction coefficient as dependent of incident irradiation energy for powders: *1* — $0.1Sn/TiO_2$, *2* — $0.5Sn/TiO_2$, *3* — $1Sn/TiO_2$, *4* — $2Sn/TiO_2$.

Table 1. Structural characteristics and band gap widths of samples

Sample	S_{sp}, m^2/g	V_{tgt}, cm^3/g	R, nm	E_g, eV
TiO_2	43.90	0.140	5.83	3.48
$0.1Sn/TiO_2$	45.65	0.200	7.91	3.31
$0.5Sn/TiO_2$	47.56	0.170	7.30	3.32
$1Sn/TiO_2$	44.25	0.163	7.40	3.33
$2Sn/TiO_2$	40.00	0.164	8.20	3.41

hancement of the particle size at tin content enhancement in the samples.

Absorption spectra of the nanocomposites (Fig. 5) show a bathochromic shift as compared with the absorption band of the pure sample. The UV-VIS spectra reveal that the absorption edge from TiO_2 to $2Sn/TiO_2$ is placed in the range of 393–410 nm (Fig. 5, a). This may indicate that tin and TiO_2 nanoparticles were integrated to form Sn/TiO_2 nanocomposites [22]. Modification of titanium dioxide with tin also leads to band gap narrowing for the composites (Fig. 5, b, Table 1), as well as to emerging of additional energy levels in the band gap of TiO_2 below the valence band that leads to sensitizing of Sn/TiO_2 composites to irradiation in the visible region of spectrum. The same band gap reduction for titanium dioxide modified with tin was observed by the authors of [1]. This is explained by insertion of Sn atoms into the titanium dioxide crystal lattice [23].

Table 2. Rate constants of photocatalytic destruction ($k_d \cdot 10^4$, s^{-1}) of dyes under UV and visible irradiation

Samples	*ST*		*RB*	
	$k_d \cdot 10^4$, s^{-1}			
	UV	VIS	UV	VIS
Without sample	0.210	–	0.17	–
TiO_2	2.215	–	1.12	–
$0.1Sn/TiO_2$	5.640	0.486	5.22	0.230
$0.5Sn/TiO_2$	5.705	0.590	5.95	0.786
$1Sn/TiO_2$	7.200	0.810	5.93	1.126
$2Sn/TiO_2$	5.630	0.470	5.09	0.710

Photocatalytic activity of the nanocomposite samples under UV irradiation increased by 2.5 times in the reaction of SF degradation and 5 times in the reaction of RD destruction compared to the pure titanium dioxide sample (Table 2).

The dyes in water solutions, as being exposed to visible light either without any catalyst, or in the presence of pure titanium oxide show no concentration changes. When the dyes in water solutions were treated with the visible light in the presence of composites, decrease of the ST and RB concentrations was observed, the rate constants of processes were dependent on the catalyst composition and structure (Table 2).

The experimental results reveal that the rate constants of photocatalytic destruction of the both dyes under UV and visible irradiation increased with icreasing of tin con-

tent in the range from $0.1Sn/TiO_2$ to $1Sn/TiO_2$ because heterojunction of two phases may act as a photogenerated electron trap and increases the lifetime of electron-hole recombination [24]. In the composite materials, the holes tend to localize on the surface of photocatalyst and may take part in the photooxidation [22]. Also, tin additives may greatly enhance the generation of hydroxyl radicals by TiO_2 [24], which results in enhancement of the photocatalytic activity. The high photocatalytic activity of the obtained nanocomposite samples seems to be connected with the decrease of the band-gap width, which was proved by the authors of [1].

In our case, addition of tin narrows the band gap of the composites as compared with the pure TiO_2 (3.48 eV); it also leads to emerging of additional energy levels in the band gap of TiO_2 below the valence band; that leads to sensitizing of Sn/TiO_2 composites at irradiation in the visible region of spectrum.

However, further enhancement of tin content in the range from $1Sn/TiO_2$ to $2Sn/TiO_2$ leads to the lower sample activity in the both reactions, because of Sn atoms can serve as electron-hole recombination centers [25] and hence the photocatalytic activity decreases. The sample $1Sn/TiO_2$ with weight content of Sn 11.43 % shows the highest photocatalytic activity in the both reactions.

Destruction of rhodamine C is accompanied with a slight (up to 5 nm) shift of the absorption band maximum to shorter waves. According to [26], such a displacement corresponds to de-ethylation of the dye molecule, mainly on catalyst surface, the process of chromophore degradation taking place basically in solution. In our case, the destruction of chromophore ring obviously prevails, which was confirmed by a drastic decrease of optical density at the absorption band maximum. Additional oxidation occurs furthermore, which is confirmed by decrease of absorption band at $\lambda < 250$ nm and by investigations of the authors of the article [27]. Any new absorption bands in the spectra of both dyes are not detected.

4. Conclusions

Mesoporous nanocomposite materials Sn/TiO_2 with different tin content were synthesized. The energy-dispersive spectroscopy based on energy-dispersive technique proves that these materials have a uniform distribution of Ti, Sn and O. The nanocomposites crystallize as anatase-type and rutile-type structures. It was established, that addition of tin to the powders led to shifting of rutile peaks to lesser angles which can be explained by the fact that Sn^{4+} ions are partially replace Ti^{4+} ions in the TiO_2 lattice. Increasing the amount of tin in composites leads to increase of the crystallite size, lattice parameters, pore radius and decrease of specific surface area and pore volume. Absorption spectra of the nanocomposites show a bathochromic shift to the long-wave range. Band-gap width of the composite materials lessens compared to the band-gap width of pure TiO_2, which may be explained by insertion of Sn atoms into titanium dioxide crystal lattice. The composite samples were photocatalytically active in the destruction of cationic dyes under UV and visible light irradiation, in contrast with pure titanium dioxide which acted as the photocatalyst only under UV irradiation. This may be attributed to the narrowing of band-gap width, participation of tin in the inhibition of electron-hole recombination, prolongation of charges lifetime, increasing of efficiency of interfacial charge separation from TiO_2 to tin and formation of doping electronic states. It was found that optimal photocatalytic activity is reached at Sn loading equal to 11.43 wt. %. Thus, the composite materials proved to be perspective photocatalysts. They could be used in environmental photocatalysis for industrial waste purification of various organic impurities, in particular, the dyes that are stable in the environment.

References

1. R.M.Mohamed, E.S.Aazam, *J.All.Comp*, **595**, 8 (2014).
2. L.Kernazhitsky, V.Shymanovska, T.Gavrilko et al., *J. Sol. State Chem.*, **198**, 511 (2013).
3. T.A.Khalyavka, E.I.Kapinus, S.V.Kamyshan, *Phys.Chem.:An Ind.J.*, **10**, 185 (2015).
4. W.Cha, S.Chin, E.Park et al., *Powd.Tech.*, **258**, 352 (2014).
5. D.Nithyadevi, R.T.Rajendrakumar, *Adv. Mater.Res.*, **678**, 373 (2013).
6. Y.Zhao, J.Liu, L.Shi et al., *Appl.Catal.B: Environ.*, **100**, 68 (2010).
7. I.Rangel-Vazquez, G.Del Angel, V.Bertin et al., *J.All.Comp.*, **643**, 144 (2015).
8. K.Vinodgopal, P.V.Kamat, *Environ.Sci.Technol.*, **29**, 841 (1995).
9. O.Carp, C.L.Huisman, A.Reller, *Prog.Sol. State Chem.*, **32**, 33 (2004).
10. T.A.Khalyavka, N.N.Tsyba, S.V.Kamyshan, *Zh. Fiz. Khimii*, **89**, 148 (2015).
11. A.Guinier, Theorie et Technique de la Radiocristallographie. Dunot, Paris (1956).

12. N.Smirnova, Yu.Gnatyuk, A.Eremenko et al., *Intern. J. Photoen.*, **2006**, 224 (2006).
13. S.Brunauer, P.H.Emmett, E.Teller, *J. Amer. Chem. Soc.*, **60**, 309 (1938).
14. E.P.Barret, L.G.Joyner, P.P.Halenda, *J. Amer. Chem. Soc.*, **73**, 373 (1951).
15. I.M.Arabatzis, T.Stergiopoulos, M.C.Bernard et al., *Appl. Catal. B: Environ.*, **42**, 187 (2003).
16. L.Andronic, A.Enesca, C.Vladuta et al., *Chem. Engin. J.*, **152**, 64 (2009).
17. J.P.Xu, S.B.Shi, L.Li et al., *J. Phys. Chem. Sol.*, **70**, 511 (2009).
18. N.Smirnova, V.Vorobets, O.Linnik et al., *Surf. Interf. Anal.*, **42**, 1205 (2010).
19. T.Hirata, K.Ishioka, M.Kitajima et al., *Phys. Rev. B: Condens. Mat.*, **53**, 8442 (1996).
20. S.Lowell, J.E.Shields, Powder Surface Area and Porosity, Chapman & Hall, London (1998).
21. K.Sing, D.Everett, R.Haul et al., *Pur. Appl. Chem.*, **57**, 603 (1985).
22. F.E.Oropeza, B.Davies, R.G.Palgrave et al., *Phys. Chem. Chem. Phys.*, **13**, 7882 (2011).
23. X.Yu, Ch.Li, H.Tang et al., *Comput. Mater. Sci.*, **49**, 430 (2010).
24. X.Li, R.Xiong, G.Wei, *J. Hazard Mater.*, **164**, 587 (2009).
25. X.L.Fu, J.L.Long, X.X.Wang et al., *Inter. J. Hydr. En.*, **33**, 6484 (2008).
26. H.Sung-Suh, J.Choi, H.Hah et al., *J. Photochem. Photobiol. A: Chem.*, **163**, 37 (2004).
27. Z.He, C.Sun, S.Yang et al., *J. Hazard Mater.*, **162**, 1477 (2009).